Separation and Purification Technology 415 (2026) 139880

Contents lists available at ScienceDirect

Separation and Purification Technology

journal homepage: www.elsevier.com/locate/seppur

A structure-based penetration model for the mechanistic interpretation of filtration regimes in baghouse needle-felt filter media

G. Kasper [*], S. Sobich, J. Meyer

Institute for Mechanical Process Engineering and Mechanics, Karlsruhe Institute for Technology, Germany

ARTICLE INFO

Keywords:
Air filtration
Baghouse filtration
Needle felts
Particle penetration
Modelling
Experimental

ABSTRACT

This study introduces a physically motivated, structure-based modelling framework for interpreting the penetration behavior of cleanable needle-felt media used in baghouse filtration. Derived from classical fibrous filtration theory, the model expresses penetration in terms of the specific fiber surface area ($\boldsymbol{S}$), a structural descriptor calculated directly from readily available media properties such as grammage and fiber fineness (dtex). It applies to the state of maximum penetration, or minimum collection efficiency, represented by new media and by regenerated media before significant filter-cake re-formation.

Penetration data for polyester needle felts from two industrial media families, examined in both new and aged states, were well described by the predicted exponential dependence

$$P = P_0 \exp(-k\boldsymbol{S})$$

wherein a single structural coordinate ($\boldsymbol{S}$) can systematically organize the experimental data and relate penetration behavior to media structure within each media family. The resulting regression parameters reflect systematic differences in filter behavior with mechanistic significance. The slope parameter (k) is interpreted as an effective accessibility or utilization factor for the internal fiber surface of the upstream layer, whereas the offset term (P_0) represents additional capture mechanisms not directly described by nominal fiber surface area, such as preferential particle capture near the outer filter surface as expected in strongly calendered or membrane-like structures, or capture in deeper regions of the needle felt.

The results show that the specific fiber surface area $\boldsymbol{S}$, derived from conventional manufacturer data, can provide a practical framework for interpreting the penetration behavior of industrial needle-felt media. Although broader validation across additional media types and operating conditions remains clearly necessary, the framework provides a practical basis for mechanistic analysis of their emission behavior in relation to media structure.

1. Introduction

Since their introduction into industrial air pollution control during the 1960s, pulse-cleaned baghouse filters have become the preferred technology for controlling particulate emissions from high-volume process industries such as cement manufacture, power generation, and metallurgical operations. Their success rests on a simple principle: unlike disposable fibrous filters, they are regenerated repeatedly by removing the deposited dust cake, allowing long-term operation under extremely high dust loads.

The filter media traditionally used for such cyclic operation are needle-felt fabrics. They have therefore evolved primarily as *cleanable surface filters*, whose performance depends not only on particle collection but also on the ability to release the accumulated dust cake during regeneration. For much of the operating cycle the filter cake itself provides the dominant filtration barrier, while the underlying needle felt merely serves as its mechanical support. Historically, improvements in baghouse emissions were therefore achieved often by increasing the interval between cleaning pulse by various operational measures.

Modern needle-felt media have nevertheless undergone considerable structural development in response to increasingly stringent emission limits and demands for improved cleanability. Finer surface layers,

* Corresponding author.
E-mail address: Gerhard.kasper@kit.edu (G. Kasper).

https://doi.org/10.1016/j.seppur.2026.139880
Received 24 June 2026; Received in revised form 2 August 2026; Accepted 23 August 2026
Available online 27 August 2026
1383-5866/

calendering, and membrane laminates have all been introduced to reduce particle penetration and facilitate cake release. Yet, somewhat paradoxically, the concept of *filter efficiency* – the central performance parameter of conventional air filtration—still plays only a limited role in the practical characterization of baghouse media. Industrial guarantees are generally expressed as absolute emission levels rather than collection efficiencies because efficiency fluctuates continuously throughout each cleaning cycle as the filter cake develops and is subsequently removed. Time-averaged emissions therefore represent the operational quantity of interest rather than a single efficiency value connected to media structure.

Nevertheless, filtration efficiency remains fundamental to understanding also the behavior of needle-felt media. Immediately after regeneration, when the protective dust cake has been removed, particles again penetrate into and through the fibrous structure until a new cake is established. The magnitude of this transient penetration determines the emission pulse characteristic of pulse-cleaned bag filters and, to a large extent, the resulting time-averaged emissions [1]. At the same time, repeated filtration cycles progressively modify the internal structure through residual dust accumulation. The penetration behavior of the clean medium therefore reflects not only its nominal structure but also its ability to capture, retain, and subsequently release particles in different regions of the felt. In this sense, the spatial distribution of particle capture is as important as the overall collection efficiency itself.

Describing such behavior quantitatively, however, is considerably more difficult for needle felts than for conventional fibrous filters. Their highly compact, anisotropic, and heterogeneous structure differs fundamentally from the loosely packed, statistically homogeneous fiber assemblies for which classical filtration theory was developed. Consequently, although needle felts are commonly distinguished in industrial practice as “coarse”, “medium”, or “fine”, these qualitative classifications reveal little about the effective filtration regime operating within the structure. What is still lacking is a simple structural framework capable of relating readily available media characteristics to penetration behavior in a physically meaningful way.

The theoretical foundations of aerosol filtration are well established. Fuchs [3] identified the principal particle-capture mechanisms of Brownian diffusion, interception, and inertial impaction, thereby providing the mechanistic basis for modern fibrous filtration theory. Building on this work, Davies [4] introduced the concept of single-fiber efficiency and derived the classical exponential expression describing the penetration of homogeneous fibrous media. His treatment established the fundamental connection between microscopic particle-capture processes and macroscopic filter performance, and it remains one of the cornerstones of filtration science. Davies also developed one of the first practically useful expressions for the pressure drop of fibrous filters, although pressure-drop behavior is outside the scope of the present work. Comprehensive reviews of the classical theory and its assumptions have subsequently been presented by Löffler et al. [5], Brown [6], and Lawrence and Liu [7].

More recently, increasingly sophisticated numerical approaches have extended these classical concepts by incorporating realistic fiber geometries and detailed flow fields. Computational fluid dynamics, reconstructed fiber structures, and multiscale modelling now permit increasingly accurate prediction of filtration performance, including the effects of compression and structural deformation in nonwoven media [8,9]. At the same time, several authors – notably Thomas and coworkers [10–12] – have demonstrated that the classical analytical framework itself remains remarkably robust when extended to account for non-ideal structural features such as mixed fiber diameters and spatial variations in packing density. These developments have substantially improved our ability to predict the performance of fibrous filter media while preserving the physical insight offered by the original analytical formulation.

The challenge posed by industrial needle felts is therefore not that they obey different filtration physics. They do not. Particle collection remains governed by the same fundamental transport mechanisms and structural features as in any other fibrous filter. Rather, the difficulty lies in translating those principles to media whose complex manufacturing process produces structures that depart substantially from the assumptions underlying classical theory. It is precisely this gap between established filtration theory and the structural reality of industrial needle-felt media that motivates the present work.

Fiber volume fractions are typically on the order of 15 to 20%, considerably higher than those encountered in conventional air filters. The manufacturing process introduces pronounced structural heterogeneity through needling, which creates preferential flow channels while simultaneously producing a highly entangled and anisotropic fiber network. In addition, needle felts are intentionally constructed from several functional layers that need not contribute equally to particle capture. The support scrim, for example, is incorporated primarily for mechanical stability, although it also limits downstream particle migration (see Appendix). Conversely, a relatively thin upstream layer of fine fibers is frequently introduced to improve cake release and reduce the accumulation of residual dust within the medium during operation [1,13].

These characteristics move industrial needle felts even further away from the classical paradigm than most disposable fibrous filters. Nevertheless, the governing filtration mechanisms remain the same. Particles are still collected by diffusion, interception, and inertial impaction, and – provided leakage is absent – the downstream particle-size distribution remains centered around the most penetrating particle size (MPPS), exactly as predicted by classical air-filtration theory [1,14]. Nor does the structural information required by the theory disappear. It is simply expressed differently. Whereas classical filtration models are formulated in terms of parameters such as fiber diameter, packing density, and layer thickness, industrial needle felts are usually specified by manufacturers in terms of grammage and fiber fineness (dtex or denier) for the individual layers. The challenge is therefore not one of fundamentally different physics, but of finding an equally meaningful structural description based on the quantities that are actually available.

One possible approach would be to reconstruct the classical description by estimating effective values of the structural parameters required for conventional fibrous-filter models. Such an approach is conceptually attractive and may provide satisfactory predictions for carefully characterized new media under controlled laboratory conditions. In practice, however, cleanable needle felts spend only a very small fraction of their operational lifetime in that state. During normal operation they undergo repeated cycles of dust deposition and regeneration, so that their effective structure evolves continuously as residual dust accumulates within the medium.

From both an operational and an environmental perspective, the most relevant condition is therefore not the average state of the filter over an entire cleaning cycle, but the reproducible condition immediately after regeneration, when the dust cake has just been removed and penetration reaches its maximum. This transient state largely determines the characteristic emission pulse of pulse-cleaned bag filters and, consequently, exerts a disproportionate influence on the time-averaged emissions of the installation. Once a new cake has formed, penetration rapidly decreases and remains comparatively low throughout most of the filtration cycle. Throughout the present work, the term *penetration* therefore refers specifically to this state of maximum penetration (minimum collection efficiency), whether for new media or for regenerated aged media before significant filter-cake re-formation.

The present study explores a deliberately simple alternative. Rather than attempting a complete structural reconstruction of needle-felt media, it examines whether the *specific fiber surface area* (***S***) calculated directly from manufacturer data such as grammage and fiber fineness, can serve as an effective macroscopic descriptor of penetration behavior. The quantity is derived from classical filtration theory, although used here in a simplified form adapted to needle felts. The study's primary purpose is not to reproduce filtration performance from first principles, but to provide a structural "coordinate" against which differences in penetration behavior can be interpreted.

The central question is therefore whether this structural coordinate can systematically organize the penetration behavior of industrial needle-felt media. If successful, such an approach would provide considerably more than an empirical correlation. It would allow the resulting model parameters to be interpreted in terms of the accessibility and utilization of the internal fiber surface, the relative importance of near-surface and/or internally distributed particle capture, and the structural changes accompanying operational aging.

Accordingly, the present work first develops the proposed structural framework and its theoretical basis. The resulting model is then applied experimentally to new and operationally aged needle felts representing two contrasting industrial media families. The objective is to test its usefulness not only as a quantitative coordinate for comparing penetration behavior, but to investigate whether it can organize that behavior in a physically meaningful manner and yield regression parameters with mechanistic significance. Broader validation across wider ranges of media structures, operating conditions, and dust properties, as well as a test of its robustness lie beyond the scope of the present study and will be addressed separately.

2. A penetration model based on specific fiber surface area

According to classical filtration theory, the particle collection efficiency of a thin fibrous layer, $\Delta c/c$, is proportional to the ratio of effective fiber cross-sectional area $\eta_F \bullet S_F$ to the total surface area S_L of that layer facing the flow,

$$\frac{\Delta c}{c} = \frac{\eta_F \bullet S_F}{S_L} = \frac{\eta_F \bullet D_F \bullet L_F}{S_L} \tag{1}$$

wherein η_F is the effective or single-fiber efficiency of a fiber of diameter D_F. L_F is the total length of fibers in that layer. These quantities are not usually specified for baghouse filter media, because media manufacturers and designers prefer to think in terms of grammage and dtex, i.e. the area weight of a media layer $\mathbf{W}_L$ (usually in g/m^2; the subscript L stands for Layer) and the fiber weight per unit fiber length $\mathbf{W}_F$ (usually in g per 10 km; the subscript F stands for Fiber).

Aside from the single-fiber efficiency η_F and a factor π, Eq. (1) is formally identical to the definition for the specific fiber surface area $\boldsymbol{S}$, i.e. the total curved fiber surface area per square meter of media surface S_L of that same filter layer:

$$\boldsymbol{S} := \frac{\pi \bullet D_F \bullet L_F}{S_L} = \frac{\pi \bullet S_F}{S_L} \tag{2}$$

Assuming cylindrical fibers, $\boldsymbol{S}$ can be derived directly from grammage and fiber fineness data normally provided by the manufacturer. These quantities, $\mathbf{W}_L$ and $\mathbf{W}_F$, are related through

$$\mathbf{W}_L := \frac{m_F}{S_L} = \frac{\frac{\pi}{4} D_F^2 \bullet L_F \bullet \rho_F}{S_L} \tag{3}$$

and

$$\mathbf{W}_F := \frac{m_F}{L_F} = \frac{\frac{\pi}{4} D_F^2 \bullet L_F \bullet \rho_F}{L_F} = \frac{\pi}{4} D_F^2 \bullet \rho_F \tag{4}$$

wherein m_F equals the mass of fiber material in that layer and ρ_F is the bulk density of the fiber material, a quantity known for most fiber materials. Rearranging and inserting these expressions into the definition for $\boldsymbol{S}$ (Eq. 2) yields

$$\boldsymbol{S} = \frac{\pi \bullet S_F}{S_L} = \frac{\pi \bullet D_F \bullet L_F}{m_F} \bullet \frac{m_F}{S_L} = \frac{\pi \bullet D_F \bullet L_F}{\frac{\pi}{4} \bullet D_F^2 \bullet L_F \bullet \rho_F} \bullet \frac{m_F}{S_L} = (4\pi)^{1/2} \frac{\mathbf{W}_L}{(\mathbf{W}_F \bullet \rho_F)^{1/2}} \tag{5}$$

When inserted back into Eq. (1), one finds that the specific fiber surface area $\boldsymbol{S}$ is proportional to the local collection efficiency $\Delta c/c$:

$$\frac{\Delta c}{c} = \eta_F \frac{\boldsymbol{S}}{\pi} = \eta_F \left(\frac{4}{\pi}\right)^{1/2} \frac{\mathbf{W}_L}{(\mathbf{W}_F \bullet \rho_F)^{1/2}} \tag{6}$$

If an infinitesimal layer is considered and the conventional negative sign is applied to the concentration decrease dc across that layer, then integration over a homogenous layer yields the classical exponential expression for the filter penetration P originally derived by Davies [4]:

$$P = exp\left\{-\eta_F \frac{\boldsymbol{S}}{\pi}\right\} = exp\left\{-\eta_F \left(\frac{4}{\pi}\right)^{1/2} \frac{\mathbf{W}_L}{(\mathbf{W}_F \bullet \rho_F)^{1/2}}\right\} \tag{7}$$

It is important to note that, up to this point, no new filtration model has been introduced. The preceding equations merely reformulate the classical penetration model in terms of structural quantities that are more readily available for industrial needle-felt media. Eqs. (6) and (7) follow directly from classical filtration theory, expressed here in terms of the structural quantities $\mathbf{W}_L$ and $\mathbf{W}_F$ which are often readily available from manufacturer specifications. Combined into the specific fiber surface area $\boldsymbol{S}$, a convenient macroscopic structural "coordinate" emerges.

Thus, once the structural coordinate $\boldsymbol{S}$ has been established, the applicability of the classical theory hinges entirely on the specification of the effective single-fiber efficiency η_F. For an idealized fibrous filter, η_F would depend only on the particle-capture physics, and hence P would be completely determined by $(\eta_F/\pi)\boldsymbol{S}$. Various expressions have been proposed for estimating η_F from non-dimensional transport parameters, particularly for interception-dominated filtration [15], these formulations have not been rigorously validated for needle-felt-like structures. For industrial needle-felt media a first-principles determination of η_F is not presently feasible. The complex fiber arrangement produced by needling, fiber entanglement, local compression, and preferential flow paths prevents reliable estimation of an effective single-fiber efficiency from the media structure alone.

The term η_F/π is therefore replaced by an empirical coefficient k representing an effective fiber-utilization or accessibility factor. This coefficient incorporates not only the particle–fiber collision physics itself, but also the effective accessibility of the nominal internal fiber surface. Accordingly,

$$P = P_0\, exp\{-k\boldsymbol{S}\} \tag{8}$$

where P_0 is an additional fitting parameter (not part of classical theory) accounting for baseline capture mechanisms not represented by the nominal specific fiber surface area $\boldsymbol{S}$. Such mechanisms may include surface compaction or membrane-like surface activity caused by calendering and will be discussed in the context of the experimental data.

Eq. (8) is therefore no longer a purely first-principles prediction, but becomes a semi-empirical expression capable of yielding experimentally meaningful values for k and P_0. Its usefulness depends on the assumption that these parameters remain sufficiently stable over a family of related media structures.

Several arguments support this assumption. Face velocities in baghouse filtration are comparatively low and usually confined to a narrow operating range of only a few cm/s. In addition, fiber diameters within a given media family often vary only moderately. Particle capture near the MPPS is therefore expected to be dominated primarily by interception, while inertial impaction and Brownian diffusion remain comparatively small [15]. This reduces the variability of η_F and supports the use of Eq. (8) as a practical framework for comparing penetration data between related needle-felt media.

3. Experimental

3.1. Filter media and structure parameters

The model is now applied to six needle felts covering a representative range of structural parameters, as summarized in Table 1. All media were mechanically bonded polyester (PET, polyethylene terephthalate) needle felts with calendered surfaces, except for the coarse medium of Group A. The media were selected from two product families originally classified only qualitatively as "coarse", "medium", and "fine", as is common industrial practice. Media in Group A were commercial off-the-shelf products, whereas those in Group B were custom manufactured for the current and related investigations. For the latter group, the surface treatment and overall grammages of the media were kept as constant as possible; only the fiber fineness was varied systematically.

Like many needle felts, the media consisted of three layers, including a support layer ("scrim") sandwiched between an upstream and a downstream fiber layer with differing grammage and fiber fineness. Table 1 summarizes the nominal layer properties provided by the manufacturers in terms of grammage and dtex.

Fiber diameters D_F and specific fiber surface areas $\boldsymbol{S}$ listed in the table were calculated from the respective properties of the upstream and downstream layers. In practical experience with modern surface-filter media, the upstream region can often be regarded as the dominant — and in some cases effectively the only — active filtration zone within the felt structure. Klingel and Löffler [13] were among the first to suggest that particle penetration and residual dust accumulation in cleanable surface filters are largely self-limiting and remain confined predominantly to the region above the support layer during stable operation. This interpretation was later refined by Höflinger [16], who showed that especially for surface-treated media, the porosity properties at and immediately below the surface are crucial for controlling particle penetration and clogging behavior. The same conclusion is supported by our own observations presented in the Appendix, where representative cross-sections illustrate both the internal fiber structure of needle felts and the limited penetration depth of deposited dust.

Therefore, the *upstream* values of $\boldsymbol{S}$ were selected as the quantitative structural coordinate to analyze penetration data for the two media families and compare them with the proposed model.

Table 1
Properties of filter materials in units as supplied. Note that grammages per layer are nominal and the sum total of all layers may differ slightly from the total grammage by weight.

	Media group A			Media group B		
	Coarse	Medium	Fine	Coarse	Medium	Fine
Grammage overall, g/m^2	350	500	550	467	554	542
Up-/downstream layer, g/m^2	123.5/123.5	186/217	227/227	188.5/188.5	232/232	226/226
Support layer, g/m^2	100	110	110	90	90	90
Fiber mass, dtex (g per 10,000 m)	1.7/1.7	1.5/3.3	0.9/3.3	3.3/3.3	1.7/1.7	1.0/1.0
Fiber diameter D_F, µm	12.5/12.5	11/24	6.6/24	24/24	12.5/12.5	7.4/7.4
Spec. fiber surface area*, m^2/m^2	28.6/28.6	45.8/36.0	72.2/37.7	31.3/31.3	53.7/53.7	68.2/68.2

* The specific fiber surface area is calculated using a mass density of 1380 kg/m^3 for polyester.

3.2. Experimental procedures

The required experimental data were obtained for new media as well as for aged media in their state of maximum filter penetration, i.e. after regeneration when the cake has been removed. Filters were always aged for 1000 filtration cycles, because this corresponds to an operational state at which dust accumulation inside the media has progressed and pulse-cleaned bag filters have usually reached reasonably stationary emission behavior [2]. It should be emphasized also that aging was stopped before a penetration measurement, the ducts were cleared, and the experiment then resumed at a far lower dust concentration than for aging, to avoid any loading, as detailed below.

Experimental procedures for laboratory characterization of cleanable filter media have been described extensively elsewhere [1,18]. Only the essential aspects are summarized here. All measurements, both for filter aging and to determine the penetration at a given filter age, were made on a filter rig according to ISO 11057 (also ASTM 6530) with coupons of 15 cm in diameter. For each grade of media these coupons were cut from the same sheet and then selected for a narrow distribution of pressure drops to ensure homogeneity.

Experiments were made at a filter face velocity of 3.33 cm/s with the test dust Pural SB™. The dust load for aging according to ISO protocols was 10 g/m^3. For concentration and size distribution measurements required to determine the penetration, the dust was highly diluted with the coarse fraction $\gtrsim$10 µm removed by sedimentation so as to (a) avoid loading the filter and thereby changing its efficiency unduly during the measurement and (b) remain within the operating range of the optical particle counter (OPC; PALAS Promo 2000 equipped with a Welas Sensor 2100; detection range 0.2 µm to 10 µm optical diameter).

3.3. Definition and measurement of penetration; particle size distributions

Comparisons with the model require a suitably averaged global penetration value P to be extracted from the experimental data, defined for the present purposes as

$$P = \frac{total\ downstream\ volume\ concentration}{total\ upstream\ volume\ concentration < 10\ \mu m}$$

Such a definition introduces an element of arbitrariness, because the choice of upstream size spectrum is ultimately arbitrary. However, the data remain intercomparable as long as the upstream reference remains the same for all measurements. This was ensured as best possible. Calculating P from the volume concentration is experimentally more demanding because volume-based size distributions are considerably noisier than their number-based equivalents. Nevertheless, this definition is operationally more relevant because industrial emission criteria are generally based on particle mass rather than particle number.

As noted above, the penetration measurements were carried out with the same test dust used to age media, but at a very low upstream concentration to avoid loading the media during a measurement (typically 5 min), and by providing sedimentation time to ensure the removal of the coarsest fraction which contributes nothing to the penetration. The upstream concentration and size distribution were kept constant as much as possible. The size distribution obtained by OPC was truncated at 10 µm (where very few particles were present) because that range corresponded well to the downstream size spectrum discussed in the following figures.

Fig. 1 shows typical downstream particle-size distributions measured for the medium-grade filter of Group A in its new and aged states. As expected, the number-based distributions are comparatively smooth and confined almost entirely to particle diameters below approximately 1 µm, i.e. close to the MPPS of the filter. The emitted size spectrum for the new filter is only slightly broader than that obtained after aging for 1000 cycles and changes very little thereafter. Conversion to volume-based distributions broadens the spectrum considerably but also increases statistical noise because the calculated particle volume is highly

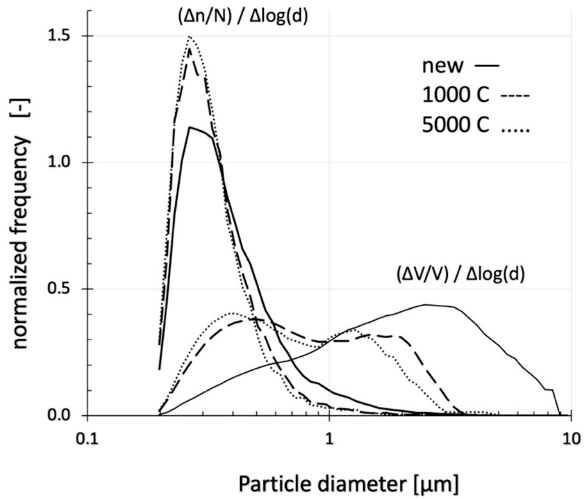

Fig. 1. Dust particle size distributions downstream of a filter (Group A, medium grade) in its new and aged states. The spectra are normalized by area and volume spectra are smoothed. The aging state of 5000 cycles is included for information to show that the size spectrum no longer changes appreciably after 1000 cycles.

sensitive to occasional counts of a few super-micron particles.

In practice, this produced occasional isolated spikes in the volume distributions even though many OPC channels above approximately 3 or 4 µm recorded zero counts during most of the measurement period and only occasional single counts otherwise. No appreciable particle mass was emitted above this size range. Although fractional penetration curves such as those shown in Fig. 2 could in principle be determined with sufficient averaging and repeated runs, obtaining complete data sets of adequate quality proved too cumbersome for the purposes of the present study. The use of total particle-volume concentration ratios therefore represented a practical compromise. Fig. 2 also justifies truncation of the upstream particle-size spectrum above 10 µm.

4. Results and physical interpretation of model parameters

4.1. Dependence of penetration on specific fiber surface area

Fig. 3 summarizes the penetration data obtained for the media of

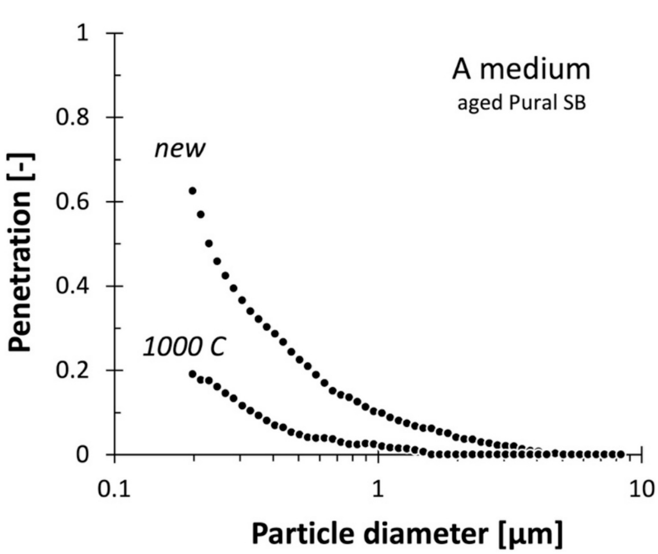

Fig. 2. Fractional penetration curves for a filter (Group A, medium grade) in its new and aged states.

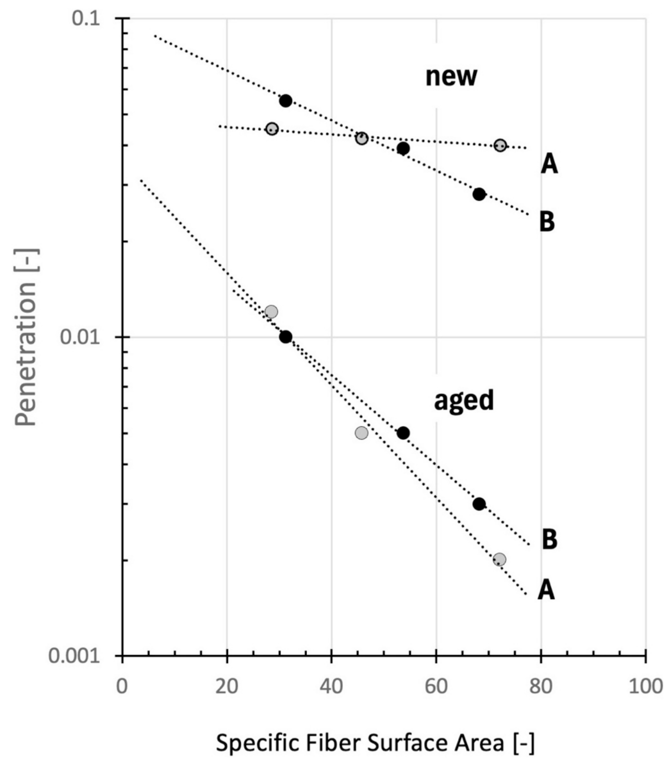

Fig. 3. Penetration vs. specific fiber surface area for media of Groups A and B.

Groups A and Group B. Penetrations of new media are typically in the range of approximately 5%, but decrease to 1% or less with operational aging due to the gradual accumulation of residual dust inside the media, reflecting the expected increase in filtration efficiency.

The measured penetration values follow the exponential dependence on specific fiber surface area predicted by the proposed framework consistently across both media families and aging conditions. Beyond the overall quality of the regressions, Fig. 3 reveals systematic features such as relative differences in slope for Groups A and B and their reversal after operational aging, which are discussed in detail below.

A comment is appropriate regarding repeatability and statistical significance. With needle felts, experimental scatter arises not only from usual fluctuations in external operating conditions or from the limited number of repeated measurements, but also from the well-known structural variability of media across the manufactured filter web itself. As mentioned earlier, this inherent material variability was reduced as much as possible by selecting coupons from within a relatively narrow band of pressure drops and area weights. Nevertheless, part of this variability inevitably carries over into the measured penetration, the aging behavior, and ultimately the fitted model parameters. Representing these different contributions by graphical error bars or confidence intervals would require a substantially broader experimental basis and, more importantly, a clear separation between measurement uncertainty and intrinsic material variability. For the purposes of the present study, emphasis is therefore placed on the systematic structural trends observed across deliberately contrasting media families rather than on statistical analysis of nominally identical specimens.

Table 2
Regression coefficients P_0 and k obtained from the data of Fig. 3.

	P_0	k
A new	0.048	0.003
B new	0.098	0.018
A aged	0.036	0.041
B aged	0.028	0.032

The regression coefficients derived from Fig. 3 are summarized in Table 2 and provide the basis for the following mechanistic interpretation of the two media families.

The two media families differ substantially with respect to both the slope parameter k and the offset term P_0, and both parameters evolve consistently also with filter aging. These systematic trends are consistent with the structural framework represented by Eq. (8) and permit a physically meaningful interpretation.

4.2. Mechanistic interpretation of P_0 and k

The offset parameter $P_0 \leq 1$ represents capture mechanisms that are not directly described by the nominal specific fiber surface area.

It can therefore provide information on contributions to particle collection that lie outside the structural coordinate $\boldsymbol{S}$. In classical filtration theory, such an offset does not exist because the penetration approaches unity ($P \rightarrow 1$) and the efficiency approaches zero ($E \rightarrow 0$) as the available fiber surface tends to zero ($\boldsymbol{S} \rightarrow 0$). In the present model, however, P_0 is not intended to represent the mathematical limit for vanishing fiber surface. Rather, it is a structural descriptor representing additional particle-capture mechanisms that operate independently of the nominal upstream fiber layer. Such mechanisms can include particle capture by deeper layers of the needle felt (i.e. below the nominal upstream layer) or on the filter face, due to surface compaction caused by calendering or when a membrane is added.

According to Table 2, the difference in P_0 between the two media families in the new state is significant (approximately a factor of 2), with new Group B media exhibiting distinctly larger P_0 values (i.e. a smaller offset). This indicates that the relative contribution associated with the accessible fiber structure of the top layer (represented by $\boldsymbol{S}$) is more pronounced in Group B. By contrast, the smaller P_0 values observed for the new Group A media suggest that additional capture mechanisms outside the idealized fibrous-filter description represented by $\boldsymbol{S}$ contribute more strongly to the overall penetration reduction.

This suggests a structural and functional difference between the two media families that is not immediately apparent from the nominal media properties listed in Table 1. For aged media, the difference in P_0 becomes smaller in relative terms, although the offset contribution itself becomes increasingly important as the overall penetration decreases. At the same time, the regression slopes evolve differently for the two groups, leading to the slope reversal discussed below.

The slope parameter k represents the effective accessibility and utilization of the internal fiber surface within the upstream filter layer. Large values of k indicate that a greater fraction of the nominal fiber surface actively contributes to particle capture – or, differently put, that adding fibers contributes more strongly to a reduced penetration – whereas smaller values reflect increasing shielding or limited accessibility of the internal structure.

The two media families thus occupy distinctly different regions of the ($P_0 k$) parameter space. Fiber accessibility appears to be substantially higher in Group B than in Group A, where portions of the internal fiber surface may be increasingly shielded from the flow field, possibly as a consequence of stronger surface compaction caused by calendering. In physical terms, a shallow slope suggests that filtration is concentrated primarily within the upper region of the top layer, while fibers located deeper within the structure contribute comparatively little to particle capture. This should be distinguished carefully from true membrane-like or outer-surface filtration, which contributes instead to the offset term P_0. Together, the two fitting parameters therefore sharpen considerably the mechanistic interpretation of the term "surface filtration".

Operational aging changes not merely the overall penetration level but the balance between the two capture mechanisms represented by P_0 and k: The slopes of A and B converge while simultaneously becoming steeper. At first sight, steeper slopes might now be interpreted as improved utilization of the original fiber surface. More plausibly, however, they result from accumulation of residual dust within the top layer, which increases the effective filtration strength[1)] of the accessible fiber structure. Since media with larger $\boldsymbol{S}$ exhibit higher initial collection efficiency, they also retain proportionally larger amounts of dust during operation. The original spread in penetration therefore becomes amplified with age, leading to steeper regression slopes.

Because the depth of dust infiltration decreases progressively with operating time as the filter approaches stabilized surface-filtration behavior, the additional capture efficiency associated with residual deposits should eventually approach a limiting state. Within the framework of the present model, this corresponds qualitatively to an increase of the slope parameter k during early aging, followed by gradual saturation, while the offset contribution P_0 decreases in relative importance as additional capture mechanisms become increasingly associated with the active upstream region represented by $\boldsymbol{S}$.

4.3. Partitioning into structure-dependent and structure-independent contributions

An additional practical value of the proposed framework is that it permits partitioning of the total penetration reduction into structure-dependent and structure-independent contributions within each media family. According to the fitted penetration model,

$$P = P_0 \exp(-k\boldsymbol{S})$$

the overall penetration P may be interpreted formally as the product of two independent contributions. Taking the negative logarithm transforms the expression into an additive representation of the logarithmic penetration reduction,

$$-\ln P = -\ln P_0 + k\boldsymbol{S}$$

The first term represents the $\boldsymbol{S}$-independent contribution, whereas the second term represents the contribution associated directly with the accessible fiber surface area $\boldsymbol{S}$. The corresponding fractional contributions are therefore

$$f_0 = \frac{-\ln P_0}{-\ln P_0 + k\boldsymbol{S}} \tag{9}$$

and

$$f_S = \frac{kS}{-\ln P_0 + k\boldsymbol{S}} \tag{10}$$

with $f_0 + f_S = 1$. The quantities f_0 and f_s represent the relative contributions of the $\boldsymbol{S}$-independent and $\boldsymbol{S}$-dependent terms, respectively, to the total logarithmic penetration reduction (an analog to "efficiency"). They provide a quantitative measure of the extent to which filter performance is associated either with additional capture mechanisms outside the nominal top-layer fiber structure or with particle capture scaling directly with the accessible internal fiber surface.

Although these quantities should not be interpreted as direct spatial measurements of particle deposition, they nevertheless sharpen considerably the mechanistic interpretation of the fitted parameters. Table 3 summarizes the resulting values of f_0 and f_s.

For new Group B media, the $\boldsymbol{S}$-dependent contribution is substantial and increases systematically with media fineness. In this sense, the penetration reduction of these media appears to be governed to a significant extent by the accessible internal fiber structure represented by $\boldsymbol{S}$. Nevertheless, the fitted offset contribution f_0 remains appreciable, indicating that additional mechanisms such as top-layer compaction (resulting in membrane-like surface activity and partial fiber shielding)

[1] For isolated fibers the capture efficiency increases particularly strongly with dust load when the bare fibers have a low capture efficiency, as is generally the case here [17] Qualitatively, this probably applies also to needle felts.

Table 3
Fractional contributions f_0 and f_s to the total logarithmic penetration reduction.

		Coarse	Medium	Fine
	S	28.6	45.8	72.2
A new	f_0	0.97	0.96	0.93
	f_s	0.03	0.04	0.07
A aged	f_0	0.74	0.64	0.53
	f_s	0.26	0.36	0.47
	S	31.3	53.7	68.2
B new	f_0	0.80	0.71	0.65
	f_s	0.20	0.29	0.35
B aged	f_0	0.78	0.68	0.62
	f_s	0.22	0.32	0.38

or particle capture in deeper regions of the needle felt seem also to contribute to the overall filtration behavior.

The situation differs substantially for the new Group A media. Here, the $\boldsymbol{S}$-independent contribution remains dominant over the entire fineness range, particularly for the coarser structures where f_0 approaches unity. Even for the finest Group A medium, the fiber-surface-related contribution remains comparatively modest. This behavior suggests incomplete utilization of the nominal top-layer fiber surface for particle capture. Additional penetration reduction must therefore arise from mechanisms localized near the outer filter surface or from structural effects not adequately represented by the nominal specific fiber surface alone.

The comparatively small slope parameter k is fully consistent with this interpretation and suggests increased shielding or reduced accessibility of fibers located deeper within the top layer.

Upon aging, the partition shifts markedly toward the $\boldsymbol{S}$-dependent contribution for both media families, particularly for Group A. This trend is mainly due to the accumulation of residual dust within the top layer, which increases the effective filtration strength associated with its fiber structure. At the same time, the distinction between Groups A and B becomes less pronounced, suggesting that the active filtration structure becomes increasingly dominated by residual dust deposits. Nevertheless, substantial f_0 contributions remain even after aging, indicating that capture mechanisms outside the idealized fibrous-filter description continue to contribute appreciably to the overall filtration behavior.

It has been emphasized that f_0 and f_s are not spatial fractions in a strict sense. Nevertheless, it is tempting to interpret them qualitatively in this manner for engineering purposes. Returning to Fig. 1, one notes that the new media of Groups A and B achieve relatively similar overall penetration values, but by rather different mechanisms. The Group A media appear to capture particles predominantly near the outer surface before they can penetrate deeply into the fibrous structure, probably due to stronger surface compaction caused by calendering. In this case, the larger offset contribution may indeed be interpreted as reflecting near-surface filtration behavior. At the same time, the relatively shallow slopes indicate comparatively inefficient utilization of the internal fiber surface.

The Group B media, by contrast, appear to utilize the accessible top-layer fiber structure more effectively and therefore rely less strongly on heavy calendering or membrane-like surface activity. Their steeper slopes suggest more effective internal filtration within the upstream layer. However, the slope reversal observed after aging indicates that progressively larger amounts of residual dust are retained inside the active structure of the B media, thereby increasing filtration effectiveness and reducing penetration further.

4.4. Comparison with classical filtration theory

Finally, one may ask whether the *original classical efficiency expression of Eq. (1)* would already suffice to explain the observed experimental trends in filter efficiency. To examine this question further, we first derive a scaling law for the efficiency E as a function of fiber diameter D_F for *new* media of approximately constant grammage. This will permit comparisons with actual efficiency data obtained from Fig. 3 for the medium and fine grades within each media family, because these pairs differ mainly in fiber diameter while their grammages remain comparatively similar (compare Table 1).

At constant grammage the total fiber length per unit filter area then scales approximately with

$$L_F \sim \frac{1}{D_F^2} \tag{11}$$

because the fiber mass per unit length is proportional to D_F^2. Furthermore, for the relatively thick fibers and relatively fine particle sizes around $1\,\mu m$ (i.e. around the MPPS) that are mainly relevant for emission, particle capture is expected to be dominated primarily by interception. In this regime, the single-fiber efficiency scales approximately with the interception parameter $R = D_p/D_F$, such that

$$\eta_F \sim R^2 \sim \frac{1}{D_F^2} \tag{12}$$

while inertial impaction and diffusion remain comparatively small [15]. Classical filtration theory would therefore predict an overall scaling with

$$E \sim \eta_F D_F L_F \sim \frac{1}{D_F^2} \bullet D_F \bullet \frac{1}{D_F^2} = \frac{1}{D_F^3} \tag{13}$$

According to Table 1, the fiber diameter ratio between the medium and fine grades is approximately 1.7 for both media groups. The classical efficiency model would therefore predict an efficiency ratio of approximately $1.7^3 \approx 4.9$.

The corresponding efficiency values can be extracted from the penetration data of Fig. 3, using the standard formula $E = 1 - P$. The respective values are 0.58 and 0.63 for Group A, and 0.61 and 0.72 for Group B, which gives observed efficiency ratios of only about 1.1 and 1.2, respectively.

The much weaker experimental dependence compared with the classical D_F^{-3} scaling indicates that only a fraction of the nominal fiber surface contributes effectively to particle capture under the conditions investigated. This behavior is consistent with reduced accessibility of the internal fiber surface arising from the complex three-dimensional structure of industrial needle felts, although the present study does not identify the individual structural mechanisms responsible.

5. Conclusions

The present study examines whether the filtration behavior of industrial needle-felt media can be interpreted within a simple structural framework based on the specific fiber surface area.

Starting from classical filtration theory, the governing expression for filter penetration was reformulated in terms of the specific fiber surface area $\boldsymbol{S}$, derived from structural quantities that are readily available from manufacturer specifications. Rather than attempting a first-principles description of the complex fiber architecture of industrial needle felts, the proposed approach introduces an empirical accessibility parameter to account for the effective utilization of the internal fiber surface.

Application of the framework to two contrasting industrial media families demonstrates that the specific fiber surface area systematically organizes the measured penetration behavior within each family. The resulting regression parameters are not merely fitting constants but acquire a clear physical interpretation. The slope parameter k reflects the effective accessibility and utilization of the internal fiber surface, whereas the offset parameter P_0 represents capture mechanisms not directly described by the nominal fiber surface area. Together, these parameters distinguish different filtration regimes and describe their systematic evolution during operational aging.

An additional practical value of the framework is that it permits quantitative partitioning of the total penetration reduction into structure-dependent and structure-independent contributions. This partitioning provides a convenient means of comparing filtration behavior within a media family and offers further insight into the relative importance of internal fiber utilization and additional capture mechanisms. The observed changes during aging are consistent with a progressive shift toward greater utilization of the internal fiber structure through residual dust accumulation.

The encouraging agreement obtained for the two media families investigated suggests that the proposed structural framework captures essential aspects of the emission behavior of industrial needle-felt media while remaining considerably simpler than detailed mechanistic models. In this regard, it provides a practical bridge between classical filtration theory and the structural reality of industrial needle-felt media, allowing readily available structural information to be interpreted in mechanistic rather than purely empirical terms.

Broader validation across additional media structures, dust types and operating conditions is nevertheless required before wider generalization can be made. Within these limits, the framework provides a practical basis for the mechanistic interpretation of industrial needle-felt filtration and for systematic comparison of media structures using readily available structural information.

Declaration of competing interest

The authors declare that they have no known competing financial interests or personal relationships that could have appeared to influence the work reported in this paper.

Acknowledgements

Authors gratefully acknowledge the financial support of the European Consortium for Filtration Technology at the KIT as well as many valuable technical discussions with its member companies. We wish to thank BWF Envirotec and Heimbach GmbH in particular for preparing the filter media. The idea of using the specific fiber surface area as a quantitative parameter for filter fineness of baghouse filter media was born out of purely empirical observations by consortium members – we can no longer reconstruct exactly by whom – that surface area correlated well with emission level.

Appendix A. Appendix

This appendix illustrates and underlines the fact that fiber arrangements inside a needle felt differ significantly from the paradigm of an ideal, random, loosely packed fiber array underlying the classical filtration theory. Average fiber volume fractions are typically in the range of 15 to 20%. Figs. A1 and A2 illustrate representative internal structures of industrial needle felts. They also show the depth of dust penetration with filter age, i.e. number of cleaning cycles.

In Fig. A1 the upper row of three SEM images shows cross-sectional views of a typical needle felt in an earlier and an advanced stage of aging, plus a membrane coated medium in an advanced stage of aging. The lower row shows corresponding dust distributions for the same locations as above. The dust distributions were obtained by energy-dispersive X-ray imaging the same fields of view with a wave length sensitive only to the particles, in this case an aluminum hydroxide scanned on the Al-K_α wavelength. Sample preparation is based on several steps which include solidification of the structure by cyano-acrylate vapor, followed by resin infiltration, cutting and polishing [19].

For the uncoated needle felts (left-hand and central panels), the SEMs visualize typical fiber orientations, but also the occasional channels created by needling, as well as the location of the scrim consisting of thick strands of fibers. After 5000 cycles, almost all the dust is still constrained to the region above the scrim. Particle found below the scrim appear to have penetrated predominantly along needle punch holes. These images show also that portions (“islands”) of the top surface are effectively sealed off due to calendering, thereby shielding parts of the fibrous structure below from direct particle penetration.

The membrane-coated medium shown in the right-hand panel of Fig. A1 exhibits no measurable particle penetration after 5000 operating cycles. Although membrane coated media were expressly not part of this study, the image is of interest because it represents an approximate limiting case of surface-dominated filtration, where particle penetration into the fibrous structure becomes almost completely suppressed due to the efficiency of the (undamaged) membrane. The needle felt becomes a mere support. In the language of the model, $P_0 \ll 1$ while $k \rightarrow 0$.

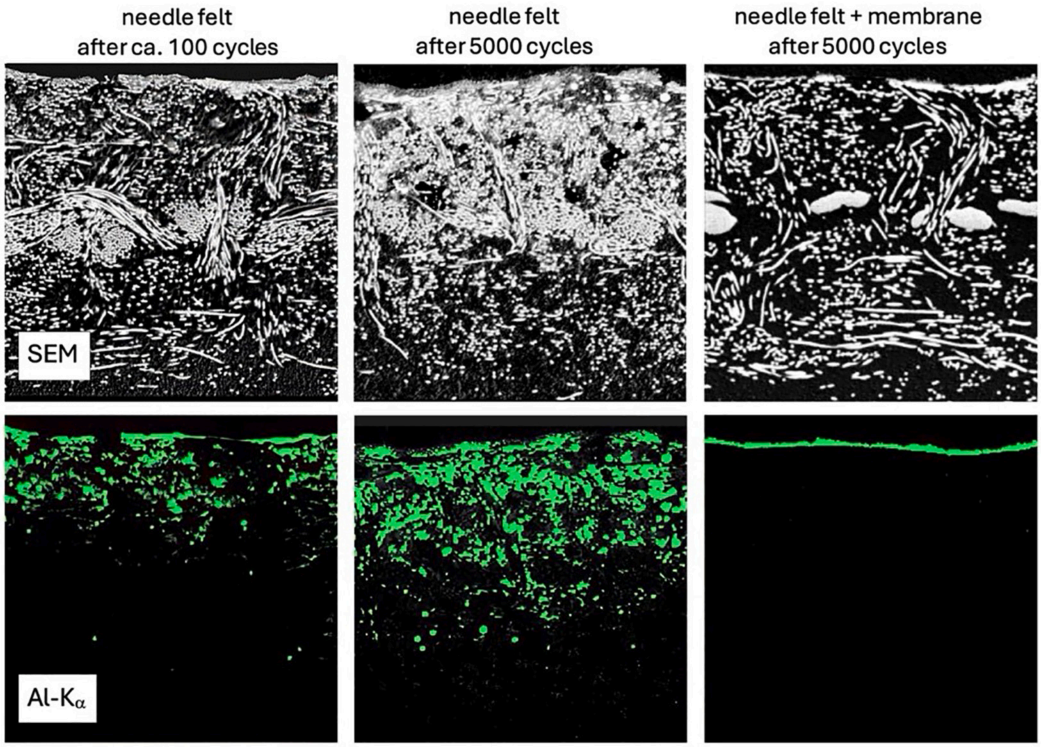

Fig. A1. Cross-sectional SEM images of PPS needle felts at different stages of aging. The upper row shows back-scatter SEM images of the fiber structure including the scrim, while the lower row shows the corresponding *Al*-K_α maps of deposited dust. The left and center columns are for a conventional needle felt after approximately 100 and 5000 filtration cycles, respectively. The right-hand column shows a membrane-coated needle felt after 5000 cycles. Flow direction is from top to bottom. The media have an approximate thickness of 2 mm.

Fig. A2 presents a higher-resolution cross-sectional SEM/EDX image of a PPS needle felt aged for 15,000 cycles. Sample preparation and *Al*- K_α imaging procedures were identical to those described for Fig. A1. The image suggests a more compact fiber structure toward the top with islands of molten polymer on the media surface resulting from the hot calender. Significant differences in local fiber orientation result from the manufacturing process typical for needle felts. The image also shows at least two microchannels. After 15,000 cycles, the dust is unevenly distributed in this cross-section, but is still constrained largely to the region near the surface. One also sees the dust infiltration along the channels and its accumulation on and around the calender islands which shield the regions below.

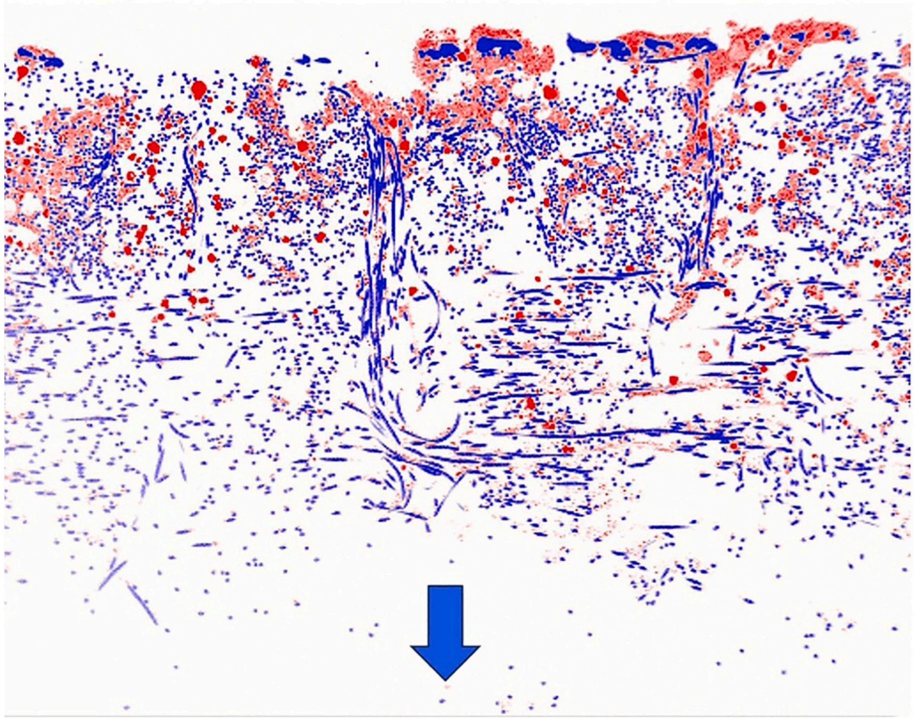

Fig. A2. Cross-sectional SEM image of a needle felt after aging for 15′000 filtration cycles with Pural SB dust. The felt structure is represented by blue fibers. Particle deposits (imaged with the aluminum K_α wavelength) are represented in red. (Cleaning pulse pressure 5 bar, filter face velocity 3.33 cm/s; flow direction represented by the arrow). Media thickness approximately 2 mm. (For interpretation of the references to colour in this figure legend, the reader is referred to the web version of this article.)

Fig. A3 shows dust penetration profiles with media depth in a typical needle felt, obtained from the *Al* K_α signal intensity. Units are arbitrary but provide a semi-quantitative measure of local dust mass due to particle infiltration. Needle felts were custom fabricated with PPS fibers, with and without support layer. Filters were aged as indicated in the figure legends for between 5000 and 100′000 cycles with Pural SB, a relatively free-flowing particle material, before cutting out samples for SEM analysis.

The comparison of dust penetration in media with and without a scrim shows that the scrim acts as an effective barrier limiting significant further particle penetration. With scrim, the bulk of the dust mass is retained inside the top fiber layer where it continues to increase slightly with filter age, while the deposit below changes very little. Evidently, some dust is retained also below the scrim. This is bound to happen over time because the total penetration of the media is never zero. A small percentage of particles pass through the filter, and of those some are retained below the scrim.

Together, the observations of Figs. A1–A3 support the interpretation that only a limited and structurally conditioned fraction of the nominal fiber surface participates effectively in particle capture within needle-felt media.

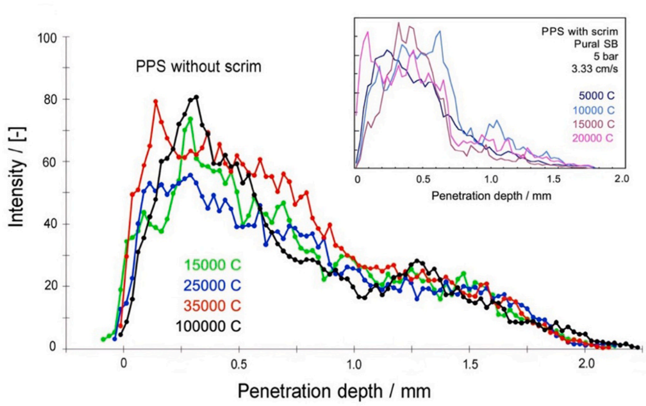

Fig. A3. Dust penetration profiles vs. media depth (where x = 0 is the upstream surface) for needle felts with and without a scrim, obtained at different filter ages (expressed as number of cleaning cycles) from the *Al*-K_α signal intensity of the particles.

The Appendix figures are based on SEM/EDX investigations carried out over several years by members of the senior author's research group during their doctoral studies. The authors gratefully acknowledge the contributions of Dr. Joachim Binnig and Dipl.-Ing. Michael Hipper to the preparation and analysis of these data.

Data availability

Data will be made available on request.

References

[1] J. Binnig, J. Meyer, G. Kasper, Origin and mechanisms of dust emission from pulse-jet cleaned filter media, Powder Technol. 189 (2009) 108–114.
[2] O. Kurtz, J. Meyer, G. Kasper, Influence of filter operating parameters on fine dust emissions from pulse-cleaned filter bags, Chem. Eng. Technol. 39 (2016) 435–443.
[3] N.A. Fuchs, The Mechanics of Aerosols, Pergamon Press, Oxford, 1964.
[4] C.N. Davies, Air Filtration, Academic Press, London, 1973.
[5] F. Löffler, H. Dietrich, W. Flatt, Staubabscheidung mit Schlauchfiltern und Taschenfiltern, Vieweg, Braunschweig, 1984; English edition: Dust Collection with Bag Filters and Envelope Filters, 1988.
[6] R.C. Brown, Air Filtration: An Integrated Approach to the Theory and Applications of Fibrous Filters, Pergamon Press, Oxford, 1993.
[7] C.A. Lawrence, B.Y.H. Liu, Relation of structure, properties and performance of fibrous media for gas filtration, Chem. Eng. Technol. 29 (2006) 957–967.
[8] O. Iliev, R. Kirsch, Z. Lakdawala, S. Rief, Modelling and Simulation of Filtration Processes, in: Large-Scale Scientific Computing, Springer, Berlin, 2014, pp. 235–244.
[9] R. Kirsch, C. Mercier, S. Antonyuk, Effects of nonwoven compression on the filter performance of air filter media, Filtr. Sep. 62 (2025) 103–110.
[10] D. Thomas, P. Penicot, P. Contal, D. Leclerc, J. Vendel, Modelling pressure drop and collection efficiency of fibrous media with mixed fiber diameters, Chem. Eng. Sci. 56 (2001) 3549–3561.
[11] D. Thomas, A. Charvet, D. Bémer, R. Régnier, Aerosol filtration modelling: effect of fiber distribution and structural heterogeneity, Chem. Eng. Sci. 59 (2004) 4263–4275.
[12] P. Contal, D. Thomas, D. Bémer, D. Leclerc, Clogging of fibrous filters by solid aerosol particles, Chem. Eng. Sci. 59 (2004) 5045–5056.
[13] R. Klingel, F. Löffler, Dust collection and cleaning efficiency of a pulse-jet fabric, Filtrat. Sep. 20 (1983) 205–208.
[14] B. Bach, E. Schmidt, Influence of leaks in surface filters on particulate emissions, J. Hazard. Mater. 144 (2007) 673–676.
[15] T. Müller, J. Meyer, G. Kasper, Low Reynolds number drag and particle collision efficiency of a cylindrical fiber within a parallel array, J. Aerosol Sci. 77 (2014) 50–66.
[16] W. Höflinger, H. Rud, G. Mauschitz, Estimation of particle penetration and dust-holding capacity of different surface-treated needle felts, Sep. Purif. Technol. 58 (2007) 256–261.
[17] G. Kasper, S. Schollmeier, J. Meyer, J. Hoferer, The collection efficiency of a particle-loaded single filter fiber, J. Aerosol Sci. 40 (2009) 993–1009.
[18] P. Gäng, Testing of cleanable filter media – status and perspectives of ISO 11057: 2011 "Test method for filtration characterization of cleanable filter media", in: Proc. AFS Adv. Filtration Technol. Conf., Louisville, KY, USA, 2017.
[19] E. Schmidt, F. Löffler, Präparation von Staubkuchen, Staub – Reinhaltung der Luft 49 (1989) 429–434. English version: Preparation of dust cakes for microscopic examination, Powder Technology 60 (1990) 173–177.